JMEPEG (2005) 14:519-527
DOI: 10.1361/105994905X56232

1059-9495/$19.00

# Mechanical Behavior of Ultrafine-Grained Cryomilled Al 5083 at Elevated Temperature

*David Witkin, Bing Q. Han, and Enrique J. Lavernia*

*(Submitted January 7, 2005; in revised form May 20, 2005)*

**The mechanical behavior of cryomilled and consolidated Al 5083 with a duplex ultrafine-grained microstructure is described for compression testing at different temperatures and strain rates. The relationship among flow stress, strain rate, and testing temperature provides an initial hotworking guide for fine-grained cryomilled aluminum alloys. The ultrafine-grained material exhibits similar deformation characteristics, such as strain-rate sensitivity, which would be expected in a conventional aluminum alloy. These findings are discussed in the context of recent empirical and theoretical models for the deformation of materials with grain sizes between 100 and 1000 nm.**

**Keywords** aluminum alloys, cryomilling, deformation mechanisms, plastic deformation, ultrafine-grained materials

## 1. Introduction

The increased strength of nanocrystalline and ultrafine-grained materials compared with their conventional counterparts offers considerable promise for their use in structural applications (Ref 1). Higher strength structural materials, for example, might be expected to be of great value in reducing component weight, which would offer designers greater flexibility in weight- or size-critical applications in aerospace or electronics. At the same time, the greater economic investment in processing necessary to produce fine-grained materials in the first place must be offset by performance to justify the adoption of new materials. For new materials to receive consideration, engineers must devise means to fabricate components with optimal properties. This includes evaluating the transformations that take place during thermomechanical processing and determining processing routes and heat treatments that result in the most favorable combination of mechanical properties.

The consolidation of nanostructured particles and powders into bulk forms has often resulted in materials with a level of residual porosity, which not only calls into question the utility of measured mechanical properties (Ref 2) but is obviously a serious impediment to adoption of these materials in load-bearing structures. In such a case, the trade-off between grain size and density might be rationalized as a means to explore mechanical behavior in a material with a truly nanocrystalline microstructure (grain size less than 100 nm). The promise of nanostructured materials as structural materials, on the other hand, can only be realized if fully dense bulk forms are produced. Studies of nanostructured materials should be pursued to understand better their behavior during forming operations. Such studies should include materials that are already fully dense or become so upon processing.

In the current study, an investigation of a bulk nanostructured Al-Mg-Mn-Cr commercial alloy (Al 5083) was conducted to understand better the transformations that occur during thermomechanical processing. The material acquired its nanostructured character through the mechanical milling of spray-atomized Al 5083 powders in a cryogenic medium, a process known as cryomilling (Ref 3, 4). The strength of bulk cryomilled aluminum-magnesium alloys was reported previously as significantly exceeding their conventional counterparts (Ref 5, 6) while maintaining acceptable ductility and fracture toughness (Ref 7). These reports were based on bulk materials that were processed by hot isostatic pressing (HIPping) of the cryomilled powders followed by extrusion. The microstructural changes that accompanied the extrusion process have been discussed in detail elsewhere (Ref 8), but the results were an increase in the average grain size and a decrease in the standard deviation of the grain size distribution in going from hot isostatically pressed (HIPped) material to extrusion. In the current study, the as-HIPped material was subjected to uniaxial compression at different temperatures bracketing the extrusion temperatures. This material has an average grain size of approximately 138 nm, which represents a grain size distribution from truly nanocrystalline to micron scale. Cryomilled powder was used to form a HIPped billet of nearly 20 kg, which is a considerable size advantage over many other powder metallurgy-based nanostructured materials. This work was performed with two objectives in mind: (a) investigating the deformation behavior of a nanostructured/ultrafine-grained alloy, and (b) determining the value of uniaxial compression testing as a proxy for other forming or hot working methods.

## 2. Experimental

The material used in this study was as-HIPped cryomilled Al 5083. The cryomilling was performed under the auspices of the Boeing Rocketdyne division. A single 20 kg powder charge of spray-atomized Al 5083 (nominal composition Al-4.4Mg-0.7Mn-0.2Cr, wt.%) was cryomilled in a circulating attritor

**David Witkin,** Department of Chemical Engineering and Materials Science, University of California, Irvine, CA 92697-2575; and **Bing Q. Han** and **Enrique J. Lavernia,** Department of Chemical Engineering and Materials Science, University of California, Davis, CA 95606. Contact e-mail: dwitkin@uci.edu.

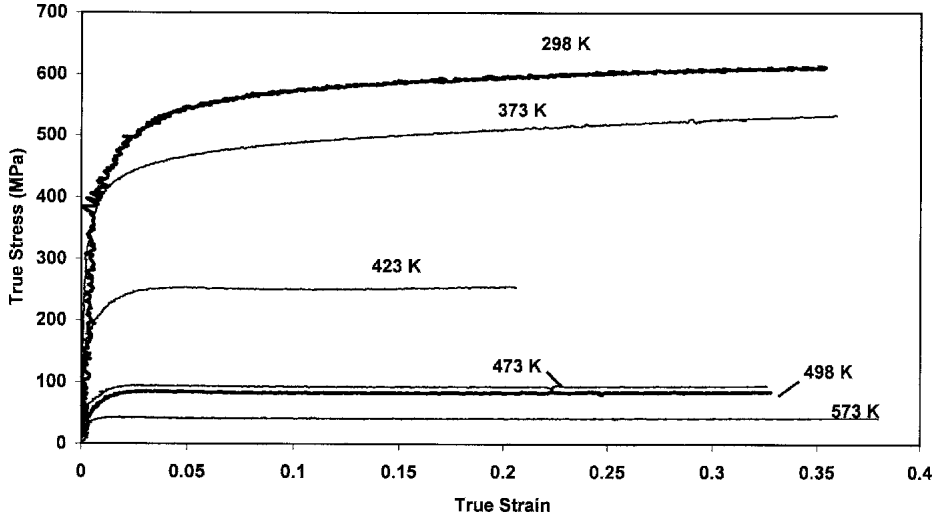


**Fig. 1** True stress-strain curves at various temperatures performed at a strain rate of $10^{-3}$ $s^{-1}$

mill with a stainless steel milling ball to powder mass ratio of 32 to 1. Stearic acid was added at a concentration of approximately 0.2 wt.% of the powder charge as a process control agent to prevent excessive cold welding of the powder particles. Liquid nitrogen was added continuously to the mill to maintain a roughly constant level of liquid nitrogen in the mill, thus creating slurry of liquid nitrogen, aluminum powder, and milling balls. The cryomilled powders were charged into an aluminum alloy can and degassed under vacuum at approximately 673 K until a vacuum level of $10^{-6}$ torr had been achieved. At the completion of the degassing cycle, the stem was crimped and welded shut, and then the can was HIPped at a temperature of approximately 600 K and chamber pressure of approximately 100 MPa.

Compression testing was performed at various temperatures between room temperature (nominally 25 °C) and 573 K on an Instron machine (model 8801) equipped with a dual-camera video extensometer. Compression samples were cylindrical with a diameter to height ratio of 1. The compression platens were lubricated with a molybdenum sulfide paste rated for use up to 673 K. For elevated temperatures, the compression specimens were allowed to soak at the testing temperature on the lower platen for about 20 min before beginning the test. The furnace temperature was controlled by a thermocouple suspended near the sample. The tests were conducted at strain rates between $5 \times 10^{-5}$ and $10^{-2} \times s^{-1}$ based on constant rates of crosshead travel and were terminated at a strain of approximately 0.25-0.30. The tests were ended at this point for several reasons. First, a nearly constant flow stress was well established at elevated testing temperatures after a strain of roughly 0.05, and at lower strains before termination the nominal strain rate would not vary too much over the course of the test. Second, some samples deformed past that amount of strain began to manifest indications of nonuniform flow, such as incipient barreling. From a practical standpoint, the limit of crosshead travel in the compression mode imposed by the apparatus (especially high-temperature platens) would have required much larger specimens to maintain an aspect ratio of unity.

The microstructures of the materials were examined using an optical microscope and transmission electron microscopy (TEM). For examination using the optical microscope, the material was first mounted in a standard metallographic mounting material, followed by hand polishing and then etching in Keller's Reagent. Thin foils for TEM examination were prepared by jet polishing disks of compression samples sectioned parallel to the compression direction. The electrolytic solution consisted of two parts methanol to one part nitric acid. The samples were polished at a temperature of approximately 238 K. The foils were examined in a Philips CM-20 operated at 200 kV.

## 3. Results

### 3.1 Mechanical Behavior

True stress-true strain curves at the different temperatures for tests performed at an initial strain rate of $10^{-3}$ $s^{-1}$ are presented in Fig. 1. These curves were corrected for machine compliance, but some differences may arise because of the use of different platens at room temperature and elevated temperatures. The testing temperatures were selected on the basis of several criteria. The first was to generate some variation in stress strain behavior. This can be seen in the work-hardening behavior exhibited by the material at testing temperatures of 373 K and room temperature. A constant flow stress is achieved at temperatures no lower than 423 K. Another purpose was to test the material at temperatures at which the as-HIPped material had been extruded under low strain rate, isothermal conditions. Extrusions had been performed previously at temperatures of 473 and 498 K with resulting differences in mechanical behavior: the material extruded at the higher temperature had roughly 40% higher elongation, but its strength was less than 5% lower in room temperature tensile tests (Ref 6). The compressive behavior of the HIPped material was very similar at these two temperatures, with the flow stress at 473 K exceeding that at 498 K by about 12%.

Analysis of the flow stress determined at 5% true strain for each temperature (obtained from the stress-strain curve intersected by a line parallel to the slope of the elastic region at an offset value of 5%) is given in Fig. 2. Here the values of flow stress ($\sigma$) are plotted versus strain rate ($\dot{\varepsilon}$). Values of the strain-rate sensitivity exponent, $m$, determined for each testing temperature according to the equation:

$$\sigma = K_1 \cdot \varepsilon^n \cdot \dot{\varepsilon}^m \quad \text{(Eq 1)}$$

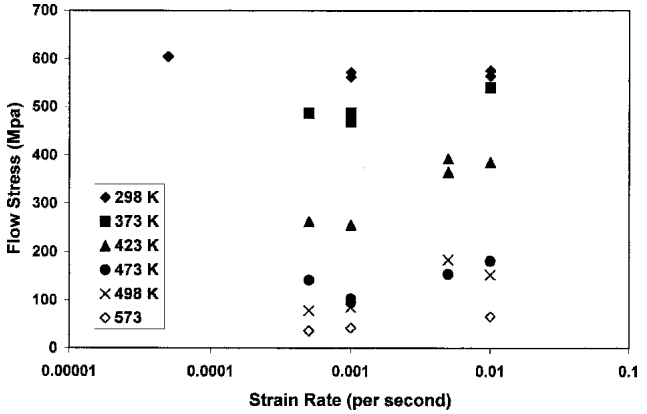


**Fig. 2** Flow stress as a function of strain rate for different testing temperatures

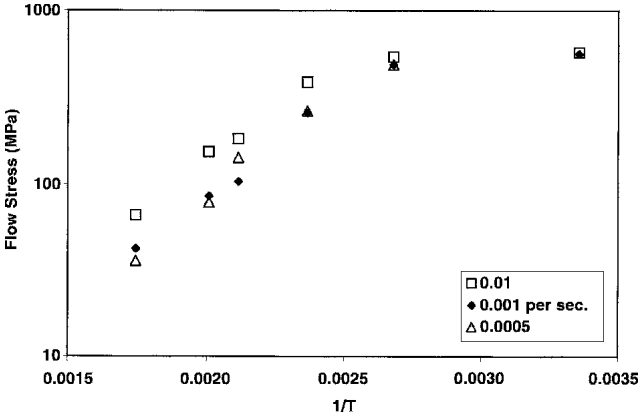


**Fig. 3** Flow stress at three different strain rates plotted as a function of reciprocal temperature

under the condition of ignoring the work-hardening behavior (*n*: stress exponent), are presented in Table 1. At room temperature and 373 K, the work-hardening behavior is evident, and there is a greater effect of strain than strain rate on the flow stress. At temperatures no lower than 423 K, the work-hardening behavior is diminished such that the effect of strain rate plays a dominant role on flow behavior. The strain-rate sensitivity exponents, without consideration of the work-hardening effect, range from slightly negative at room temperature to between 0.15 and 0.28 at elevated temperatures. The low values at room temperature and 373 K correlate with the observed work-hardening behavior in the stress-strain curves, whereas higher values occur where steady-state flow stress is achieved. The relationship between flow stress and temperature, at a constant level of strain and strain rate, can be expressed by Eq 2:

$$\sigma = K2 \exp[QRT]\varepsilon,\varepsilon \quad \text{(Eq 2)}$$

where $K_2$ is a constant different from that in Eq 1, $Q$ is the activation energy for plastic flow, $R$ is the universal gas constant, and $T$ is the testing temperature (Ref 9). For each strain rate, the flow stress at 5% plastic strain is plotted in Fig. 3 as a function of the inverse of temperature. In a semilogarithmic plot, the linear behavior of $\sigma$ versus $1/T$ would be expected if the materials exhibited similar deformation characteristics, which could be explained by a single value for activation energy. As expected, however, at lower testing temperatures, where $m$ takes on a lower value, the plots deviate from a linear trend. At temperatures of 423 K and above, however, the slopes of the curves do not differ greatly over two orders of magnitude of strain rate, yielding average activation energy of approximately 25 kJ/mol.

**Table 1 Strain-rate sensitivity exponents**

| Testing temperature, K | *m* |
|---|---|
| 298 | –0.01 |
| 373 | 0.04 |
| 423 | 0.16 |
| 473 | 0.15 |
| 498 | 0.28 |
| 523 | 0.20 |

### 3.2 Description of Material

Cryomilled aluminum-magnesium alloy powders typically have average grain sizes of 20-25 nm, whereas the particle size is on the order of 30 or 40 μm (Ref 4, 10). Unlike spray-atomized particles, which are spherical, the cryomilled powders are blocky and angular (Ref 4), a fact that should not affect the densification process during HIPping (Ref 11). The density of the as-HIPped material and several deformed specimens was measured using an analytical balance equipped with an Archimedes-method kit. The density of all samples was greater than 99.8% of theoretical value for Al 5083 (2.66 g/cm$^3$), and the compression testing increased the density of the deformed material relative to the as-HIPped by less than 0.1%. During consolidation by HIPping, the bonding of particles is accomplished by various phenomena, including plastic deformation and flow and diffusive mass transport (Ref 12), but the interparticle volumes will be filled to some extent by material that does not share the same processing history as the interior of the particles, independent of the microstructural changes that occur within the particles. The duplex nature of this microstructure is best illustrated by an optical micrograph of the HIP material after polishing and etching (Fig. 4). The light-colored regions in the optical image are the coarse-grained interparticle regions, whereas the dark regions are the fine-grained microstructure of the powder particles. Using the comparison procedure for estimating area fractions (ASTM Standard E 1181-87, "Standard Test Method for Characterizing Duplex Grain Sizes"), the coarse-grained sections are estimated to constitute approximately 15% of the overall material volume. The plastic deformation during the HIPping process has effectively eliminated much of the particulate nature of the bulk material by interrupting prior particle boundaries, yet the former interparticle regions are still in evidence. Based on examination of several TEM images and statistical measuring of individual grains, the average grain size of the fine-grained matrix was 138 nm.

Examples of the microstructure after deformation are shown in Fig. 5 and 6. Both figures are taken from samples sectioned parallel to the direction of applied load. The sample deformed at room temperature to a strain of 0.30 is shown in Fig. 5. The

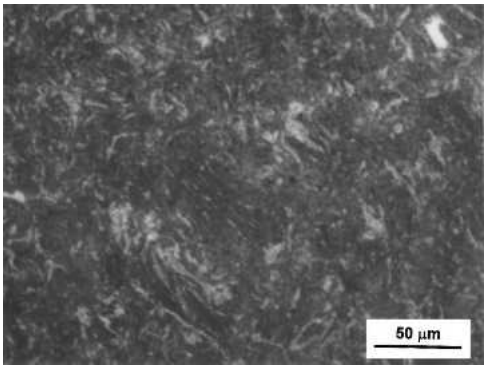


**Fig. 4** Optical micrograph of HIP material showing duplex microstructure

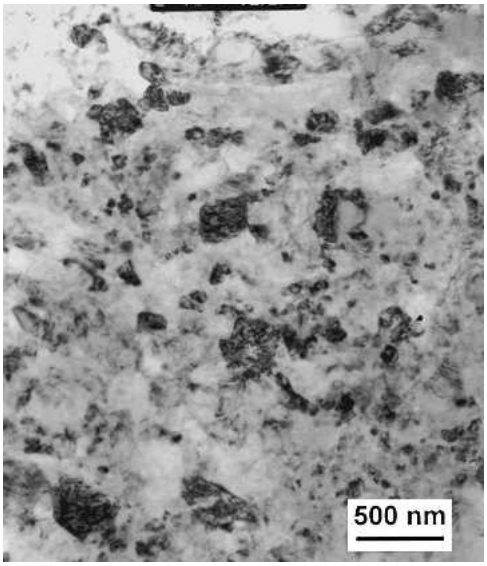


**Fig. 5** Example of room temperature deformation to a strain of 0.30

microstructure in Fig. 5 is actually similar to that in the undeformed as-HIPped material, but the interiors of the coarse grains contain tangles of dislocations, which do not appear in the fine grains. In addition, the coarse-grained regions between former prior particle boundaries show evidence of dislocation accumulation at the grain boundaries within these regions. This persists at higher deformation temperatures, as in a dark field image of a relatively coarse grain (approximately 1000 nm diameter) from a sample deformed at 423 K to a strain of 0.20, which shows that dislocation entanglement is concentrated near grain or subgrain boundaries (Fig. 6). The coarse-grained regions in samples deformed at higher temperatures show evidence of dislocation arrays, as pictured in Fig. 7, taken from a sample tested in compression at 498 K. These dislocation structures were not noted in TEM samples tested at temperatures in which grain-boundary dislocation accumulation was found.

## 4. Discussion

### 4.1 Overview of Mechanical Behavior

The mechanical behavior of the HIPped material in compression clearly exhibits a temperature-dependent change between 373 and 423 K. This change is manifest at different scales. The absence of strain hardening in compression above 373 K indicates a transition from favoring of dislocation generation and accumulation over recovery at the lower temperatures to an apparent balance between them at higher temperatures. The strain-rate sensitivity exponent increases from a negative value at room temperature to a small positive value at 373 K and then to intermediate values at the higher temperatures. Finally, there is a break in slope between these two temperature regions in an Arrhenius plot of the flow stress. Each of these aspects of the mechanical behavior will be discussed with respect to the microstructural evidence.

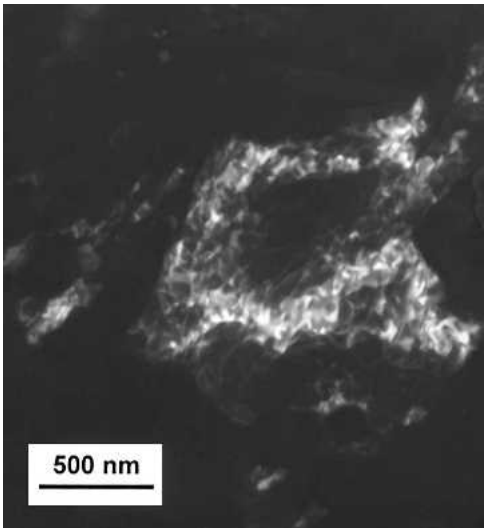


**Fig. 6** TEM dark field image of a large grain showing diffraction contrast between grain interior and grain boundaries

The nature of plastic deformation at fine grain sizes has been discussed extensively. The bulk cryomilled Al 5083 can be classified as ultrafine grained based on its grain size. This grain size regimen, which can be approximated as representing grain sizes between 100 and 1000 nm, can be considered a transition grain size between nanocrystalline grain sizes large enough to support dislocation-based plasticity (Ref 13-16) and conventional grain sizes that are dominated by intragranular Frank-Read sources. Grain boundaries have been proposed as both sources and sinks of dislocations at fine grain sizes based on molecular dynamics (Ref 17), in-situ TEM observations of deformation (Ref 18), and by noting the absence of dislocation activity in TEM investigation of deformed specimens (Ref 19). The evidence of low activation volume in cryomilled ultrafine-grained aluminum alloys extrapolated from strain-rate jump tests (Ref 20) also suggests that grain boundaries act as sources and sinks of dislocations during plastic deformation. This leaves the question of the range of grain sizes over which grain boundary sources are operative compared with conventional, coarse-grained intragranular dislocation sources such as Frank-Read sources.

Determination of this transition grain size was summarized neatly by Cheng et al. (Ref 19) as dependent on the answer to two questions: (a) whether sufficient intragranular dislocation sources exist in the material, and (b) whether the applied stress is large enough to activate those sources. Conventional behavior would be expected with affirmative answers to both questions, but the transition from grain boundary sources to intragranular sources could be expected over a range of grain sizes

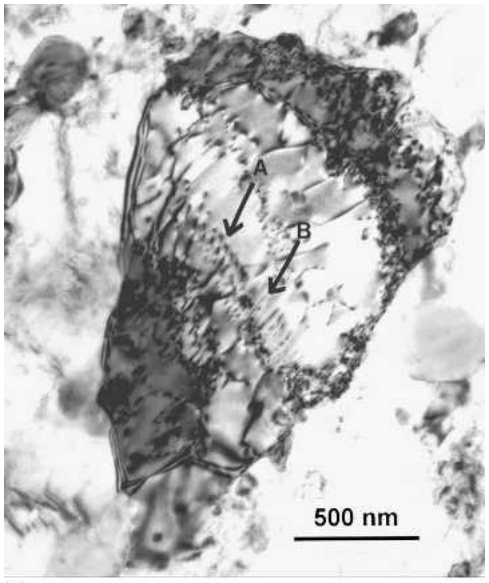


(a)

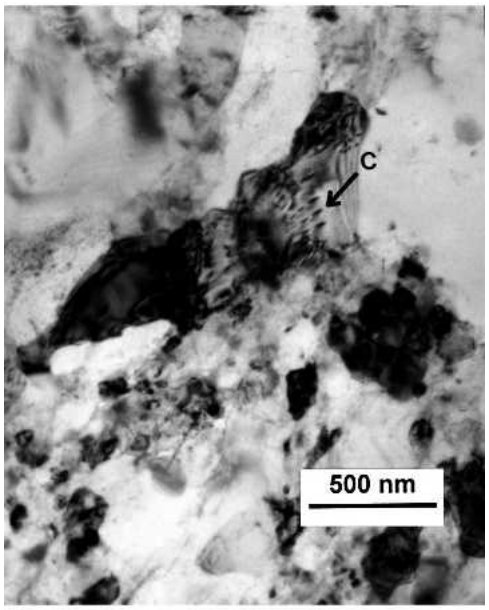


(b)

**Fig. 7** Dislocations arrays in two coarse grains from a sample deformed at 498 K

(Ref 21). The mechanical behavior based on dislocation source arguments has been divided on this basis into four regimes: the finest grain sizes, where dislocation activity is absent (<10 nm); a nanocrystalline regimen in which partial dislocations are active [roughly 10-30 nm in face-centered-cubic (fcc) metals]; intermediate grain sizes (30-1000 nm), where grain boundaries dominate as dislocation sources and sinks; and finally the conventional range, where intragranular sources dominate (Ref 22-24). A similar division for grain-size-dependent deformation behavior has been advanced based on consideration of the kinetics of plastic deformation. For fcc copper, for example, grain sizes between 10 and 1000 nm, the controlling mechanism was grain boundary shear promoted by dislocation pileups within grains, which would lead to stress concentration within the grain boundaries (Ref 23). The relationship between mechanical behavior and grain size was predicated upon the role that grain dimensions may play in the number of dislocations in a pileup and the proportion of atoms found in grain boundaries, whereas for grain sizes above 1 μm, the grain size would determine the number and mobility of dislocations, and their interaction would control plasticity (Ref 23). The exact demarcation of each regimen was considered to be a function of temperature and strain rate. Wei et al. (Ref 24) have argued that the transition from grain interior dislocation interaction to grain boundary control will be marked by a change in the average spacing between two obstacles restricting dislocation movement. At larger grain sizes, this obstacle spacing is proportional to $\rho^{-1/2}$, where $\rho$ is the dislocation density; at smaller grain sizes the obstacle spacing is directly proportional to the grain size. From this reasoning, the authors derived a mathematical expression that explained the increase in strain-rate sensitivity exponent with decreasing grain size for fcc nickel and copper (Ref 24). These arguments indicate that an intermediate grain-size regimen exists, but the exact bounds for this regimen are not established and are dependent on the material, its inherent physical properties, and its processing history as well as the imposed testing conditions, such as temperature and strain rate.

There are limited experimental data available on strain-rate sensitivity for nanocrystalline or ultrafine-grained metals, and few of these are for aluminum alloys. Al-4.0Cu-0.5Zr processed by equal-channel angular pressing (ECAP), for example, had a room temperature strain-rate sensitivity exponent of 0.005 (Ref 25). A small positive strain-rate sensitivity exponent was reported for electron-beam-deposited Al-1.5Fe with a grain size of less than 100 nm, but a numerical value for $m$ was not reported (Ref 26).

There are other fine-grained aluminum alloys for which strain-rate sensitivity values have been reported, such as rapidly solidified dispersion-strengthened alloys. At room temperature, these values are typically less than 0.05, and they do not vary greatly at temperatures up to 673 K, although obvious trends with temperature may occur (Ref 27, 28). A minimum in $m$, including negative values, occurred at about 423 K. A similar trend was found for three conventional aluminum-magnesium alloys (5053, 5083, and 5154), with the minimum value occurring between 350 and 400 K, somewhat lower than the rapidly solidified alloys (Ref 29). The strain-rate sensitivity exponent of the cryomilled Al 5083 derived from the compression data does not show such a minimum, increasing from a negative value at room temperature to values at elevated temperatures, which are consistent with reported values for conventional Al 5083 at different temperatures (Ref 29). The strain-rate sensitivity exponent of cryomilled Al 5083 was measured previously using strain-rate change tensile tests, in this case for material that was extruded from the as-HIPped material in this study (Ref 20). In the strain-rate change tests, $m$ was reported as less than 0.01 at room temperature and approximately 0.14 at 423 K, in contrast to compression testing at different strain rates that yields −0.01 and 0.16 at these two temperatures, respectively. The similarity of these occurs despite differences in the imposed stress state (compression versus tension), differences in processing history (as-HIPped versus extruded), and the means to determine the value of $m$ (plot of $d\ln\sigma/d\ln\dot{\varepsilon}$ versus strain-rate jump). Both tension and compression testing thus yield values that are similar to the values for conventional Al 5083 (Ref 29), despite the smaller grain sizes and the presence of a negative $m$ at room temperature in

the cryomilled material. This contrasts with the trend reported for fine-grained nickel and copper (Ref 24), in which *m* showed a clear trend of increasing with decreasing grain size.

There are several differences between the cryomilled Al 5083 and the nanocrystalline and ultrafine-grained nickel and copper, which should be pointed out. First, room temperature mechanical testing of nickel, copper, and Al 5083 occurs at homologous temperatures of 0.17, 0.22, and 0.35 $T_m$, respectively. Conrad's analysis of deformation kinetics in copper was restricted to data collected below 0.25 $T_m$ to reduce the influence of lattice diffusion on the kinetics (Ref 23). The equivalent temperature in Al 5083 would be approximately 215 K, where conventional Al 5083 has a higher strain-rate sensitivity exponent than at room temperature (Ref 29). Second, as discussed, the cryomilled Al 5083 has a heterogeneous microstructure, consisting of a range of nanometer and ultrafine-grained sizes, as well as coarse-grained regions that arise during HIPping. Although the smaller grain sizes in the distributions would deform according to the grain boundary source hypothesis in the empirical model and the intermediate regimen in the kinetics-based model based on the grain size alone, much of the microstructure falls into the ambiguous region, where proponents of the respective models have invoked processing conditions and testing conditions as being as important as grain size.

### 4.2 Deformation Mechanisms in Cryomilled Aluminum Alloys

Hayes et al. (Ref 20) used the values of activation volumes calculated from strain-rate jump tests to argue that the deformation mechanism in cryomilled aluminum was more likely to arise because of grain-boundary sources and sinks than forest dislocation interactions. These materials also exhibited microstructural heterogeneity, as differences in the average grain size were mostly determined by the relative abundance of coarse-grained regions. The activation volumes and strain-rate sensitivity exponent did not show obvious trends with respect to the microstructural variation, but cryomilled commercial purity aluminum and Al 5083 had opposite trends in activation volume and strain-rate sensitivity with respect to temperature. For aluminum, the activation volume increased and *m* decreased after increasing the testing temperature from room temperature to 423 K; for Al 5083, the trend was the opposite. Opposing trends in strain-rate sensitivity and activation volume are to be expected based on the inverse relationship between them (Ref 30). At the same time, in coarse-grained materials deforming by forest dislocation interaction, activation volumes are expected to increase with increasing temperature, at least at temperatures up to 0.22 $T_m$ (Ref 23). A decrease in activation volume was noted for fine-grained copper up to 0.28 $T_m$, consistent with a stress concentration at grain boundaries caused by dislocation pileups in grain interiors (Ref 23). The implication is that cryomilled Al 5083 is exhibiting behavior consistent with coarse-grained materials, whereas the cryomilled aluminum is behaving more like an intermediate regimen material. Because these models were formulated on the basis of a different material at a specific restricted low temperature range, they are not expected to apply directly to the cryomilled aluminum. Rather, they are used to illustrate that the opposing trends of aluminum and Al 5083 suggest different dislocation-based deformation mechanisms.

The question of which deformation mechanisms are operative at which temperatures might be resolved if a specific thermally activated change were occurring. The Arrhenius plot (Fig. 3) suggests that activation energy ($Q_{def}$) for deformation at 423 K (0.49 $T_m$, where $T_m$ is the incipient melting point of Al 5083, 863 K) and above may be calculated. The value from these plots, roughly 25 kJ/mol, is well below the literature values for aluminum lattice and grain boundary self-diffusion as well as magnesium diffusion in an aluminum lattice (Ref 31, 32). Based on this comparison, it would appear that the analysis of deformation kinetics predicated on an absence of lattice diffusion would appear to be valid. Although diffusion may not be indicated by the activation energy, the value of $Q_{def}$ calculated from the Arrhenius plot is similar to that determined for the movement of vacancies or the interaction of magnesium solute atoms and gliding dislocations in studies of dynamic strain aging in aluminum-magnesium alloys (Ref 33, 34). The discrepancy between measured activation energy and those for lattice and grain boundary diffusion has also been noted for Al-6.2Zn-2.5Mg, in which an activation energy of 19.7 kJ/mol was determined (Ref 35). This value was calculated from an Arrhenius expression that included the critical strain to the onset of serrated flow and the strain rate, and the activation energy was given as the addition of separate terms for vacancy formation and migration. Hence, it was argued that the low value of activation energy reflected only the migration portion, as the number of quenched-in vacancies would reduce the need for vacancy formation in dynamic strain aging (Ref 35). Equation 2, on the other hand, was evaluated at constant strain and strain rate to give the value 25 kJ/mol. The similarity in activation energy values may be a coincidence, however, as the microstructural data for the cryomilled Al 5083 indicate that several phenomena are occurring, including grain growth and precipitation of nanometer scale secondary phases, which is restricted to the coarser grains (Ref 8). These precipitates are more abundant in samples deformed at elevated temperature than in the as-HIPped material and samples deformed at room temperature. Both grain growth and precipitate nucleation and growth might be explained by the movement of magnesium in association with dislocation and grain boundary movement. Nevertheless, calculation of activation energy is predicated on the occurrence of a single thermally activated process; this is not assured by the data at hand.

A better approach to understanding the deformation behavior is to incorporate the dependence of flow stress on both temperature and strain rate, usually in a form along the lines of (Ref 9).

$$\sigma = f(\dot{\varepsilon} \exp\left(\frac{\Delta Q}{RT}\right) \quad \text{(Eq 3)}$$

The particular approach used for the data on cryomilled Al 5083 is taken from Kocks and Meckin (Ref 36), in which the activation energy is expressed as a function of the flow stress according to:

$$\frac{\Delta G}{\mu b^3} \equiv \frac{kT}{\mu b^3} \ln\left(\frac{\dot{\varepsilon}_0}{\dot{\varepsilon}}\right) = f\left(\frac{\sigma}{\mu}\right) \quad \text{(Eq 4)}$$

where $\dot{\varepsilon}_0$ is a reference strain rate determined to be $10^7$ $s^{-1}$ for pure fcc metals. Values for temperature adjusted shear modulus $\mu$ are based on the formula given by Frost and Ashby for pure aluminum (Ref 32). Mathematically, Eq 4 is comparable to the formulations of Sellars and Tegart of the high-stress exponen-

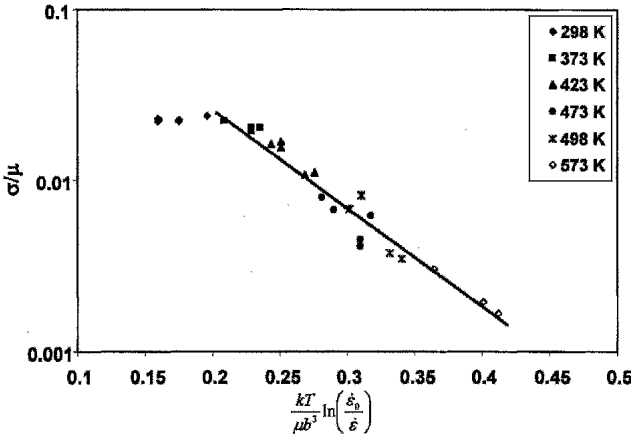


**Fig. 8** Normalized flow stress as a function of normalized activation energy of deformation and strain rate based on compression data taken at 5% plastic strain

tial relationship among strain rate, flow stress, and temperature (Ref 37). A semilogarithmic plot of normalized flow stress versus the product of the normalized activation energy combined with the strain rate thus shows the dependence of the activation energy on the flow stress. The data from the cryomilled materials in compression, taken at 5% plastic strain, are plotted according to this relationship in Fig. 8. In this plot, a straight line fits all of the data points measured at temperatures of 373 K and above with a high correlation coefficient ($r^2$ = 0.95). Although the exact value of the activation energy cannot be determined based on this presentation of the data, the straight-line fit indicates that the flow stress can be related to both temperature and strain rate at elevated temperatures. From this functional relationship, hot working conditions may be estimated for operations such as extrusion, rolling, and upset forging, albeit with the explicit caveat that the data were collected at strain rates considerably lower than those used in conventional industrial processes. For lower strain rate processes, this plot represents an initial effort to rationalize the processing of bulk cryomilled material. In addition, given the similarity noted between the strain-rate sensitivities of the cryomilled material and conventional material (Ref 29), this relationship may be generally applicable to ultrafine-grained aluminum and not just cryomilled aluminum.

At the same time, this plot does not explain the nature of the deformation and the dislocation mechanisms at work. In particular, the duplex microstructure of the HIPped material leads to the possibility that deformation may occur by a different mechanism in different grains or regions. This type of scenario was proposed for a ball-milled, ultrafine-grained/nanocrystalline zinc, in which the nanocrystalline region appeared in TEM to be undeformed even after tensile strains exceeding 1.0, suggesting grain boundary sliding, whereas the stress exponent from strain-rate jump tests was consistent with dislocation climb (Ref 38). The considerable tensile strains achieved were attributed to this contribution from ultrafine grains. A similar proposal for grain-size-specific deformation mechanisms was given previously for superplastic alloys resulting from consideration of grain size distribution (Ref 39). In this case, grain boundary sliding was considered the operative mechanism in fine grains, whereas power-law creep occurred in coarse grains. In an ultrafine-grained copper with a bimodal grain size distribution, deformation twinning and stress accommodation in the coarser grains led to enhanced ductility and strain-hardening capacity (Ref 40, 41). Of particular note is the similarity of the compression stress-strain behavior of the bimodal copper (Ref 41) and the cryomilled Al 5083 HIP material, as both show similar strain-hardening behavior despite the presumed absence of twinning in the cryomilled aluminum.

### 4.3 Dislocation Mechanisms in Cryomilled Aluminum Alloys

The absence of dislocation activity in the grain interiors of deformed specimens of nanostructured and ultrafine-grained materials in general (Ref 21) and in cryomilled aluminum in particular (Ref 42) when examined using TEM has been cited a posteri as consistent with grain boundary sources and sinks for dislocations and absence of strain hardening. Dislocations are found, however, in coarse grains. Three dislocation arrays are pointed out in Fig. 7(a) and (b) within coarse grains from a sample deformed at 498 K. These arrays are tentatively described as dislocation pileups because each has closer spacing of individual dislocations at one end, and each has a plausible source and obstacle to motion, either an interior second-phase particle or a grain boundary. There are several reasons to make only a tentative designation of these arrays as pileups. First, they occur in an fcc metal with a high stacking fault energy, so that cross-slip would be expected. Second, the strain-rate sensitivity exponent at the deformation temperature gives a stress exponent of approximately 5, so that climb around obstacles might be expected as well. Third, a Burgers vector for these arrays was not determined, primarily because of the complexity and scale of the microstructure. Finally, the assumption is made that the array as it appears is a feature of deformation and not the result of relaxation after unloading and sample quenching as well as TEM foil preparation. Although the spacing between individual dislocations does vary, it does not vary significantly, so the arrays might also be interpreted as subgrain boundaries. Nevertheless, if the three arrays in Fig. 7 are treated as single pileups under load, the spacing between the source and the obstacle can be approximated by (Ref 43):

$$l = \frac{\mu Nb}{\pi(1-\nu)\sigma} \quad \text{(Eq 5)}$$

Using the temperature-adjusted shear modulus at 498 K equal to $2.25 \cdot 10^{10}$ Pa, $\nu = 0.3$, $\sigma = 85$ MPa based on the compression test, and $N = 12$, 7, and 4 dislocation lines for arrays A, B (Fig. 7a), and C (Fig. 7b), respectively, the resulting corresponding values for $l$ are 413, 240, and 140 nm. The values are very close to the dimensions in Fig. 7, raising the possibility that the value of the flow stress is determined by the size of the coarse grains and the relative density of the precipitates or obstacles within them.

## 5. Conclusions

The consolidation of cryomilled Al 5083 powders by HIPping leads to an essentially fully dense material with a duplex microstructure. The fine-grained portion of the material has an ultrafine grain size, so that a deformation mechanism largely dictated by grain boundary dislocation sources and sinks is expected. The measured strain-rate sensitivity exponents, however, are consistent with literature values for conventional Al

5083 over a range of temperatures, which presumably contain intragranular dislocation sources and deform by cutting of forest dislocations.

This contradiction may be mitigated somewhat by a primary role for the micron-scale coarse grains that are found in the cryomilled material. These grains show evidence of considerable dislocation activity, unlike the fine grains. Features that are tentatively identified as dislocation pileups within the coarse grains have dimensions consistent with the flow stress at one of the testing temperatures. The duplex microstructure can give rise to complementary deformation mechanisms occurring at the two size scales within the material, which has been suggested previously for fine-grained and superplastic materials. Consequently, dislocation evidence is observed in TEM in coarse grains but not in fine grains, although the fine grains themselves are of a size sufficient to support grain boundary dislocations.

The flow stress at different temperatures can be subjected to Arrhenius-type analysis, yielding a value for the activation energy of deformation, but it is not apparent that this is a true activation energy. By normalizing the flow stress and activation energy, however, a relationship among flow stress, temperature, and strain rate has been derived. Such an analysis does not yield an actual activation energy value, but it allows data from different temperatures and strain rates to be plotted on a single trend. Although the Arrhenius plot was consistent with the compression stress-strain curves in indicating a change in behavior between 373 and 423 K, the approach using normalized values indicated that a single relationship could relate flow stress with temperature and strain rate above room temperature. This relationship is a first step at rationalizing the deformation behavior of the cryomilled Al 5083 in a way that may be useful for slow strain-rate-forming operations. It also hints at more of a continuum in deformation behavior of the cryomilled aluminum at different temperatures than a sharp transition as indicated by strain hardening behavior and strain-rate sensitivity alone, a concept that will be useful for correlating deformation mechanisms with temperature, strain rate, and grain size.

## Acknowledgment

This work was made possible in part by the financial support of the Office of Naval Research, under contract N00014-03-C0163, with oversight by Mr. Rodney Peterson, Naval Surface Warface Center, Carderock.

## References

1. C.C. Koch, *Nanostructured Materials: Processing, Properties and Potential Applications,* Noyes Publications/William Andrew Publishing, Norwich, NY, 2002, p 1-612
2. P.G. Sanders, C.J. Youngdahl, and J.R. Weertman, The Strength of Nanocrystalline Metals with and without Flaws, *Mater. Sci. Eng. A,* Vol 234-236, 1997, p 77-82
3. M.J. Luton, C.S. Jayanth, M.M. Disko, S. Matras, and J. Vallon, Cryomilling of Nanophase Dispersion Strengthened Aluminum, *Mater. Res. Soc. Symp. Proc.,* Vol 132, 1989, p 79-86
4. F. Zhou, R. Rodriguez, and E.J. Lavernia, Thermally Stable Nanocrystalline Al-Mg Alloys Powders Produced by Cryomilling, *Mater. Sci. Forum,* Vol 386-388, 2002, p 409-414
5. B.Q. Han, Z. Lee, S.R. Nutt, E.J. Lavernia, and F.A. Mohamed, Mechanical Properties of an Ultrafine-grained Al-7.5Mg Alloy, *Metall. Mater. Trans. A,* Vol 34, 2003, p 603-613
6. D. Witkin and E.J. Lavernia, Processing Controlled Mechanical Properties and Microstructures of Bulk Cryomilled Al-Mg Alloys, *Processing and Properties of Structural Nanomaterials,* L.L. Shaw, C. Suryanarayana, and R.S. Mishra, Ed., TMS, Chicago, 2003, p 117-124
7. P.S. Pao, H.N. Jones, and C.P. Feng, Fatigue Crack Growth and Fracture Toughness in Bimodal Al 5083, *Mechanical Properties of Nanostructured Materials and Nanocomposites,* I. Ovid'ko, C.S. Pande, R. Krishnamoorti, E.J. Lavernia, and G. Skandan, Ed., Materials Research Society, Vol 791, 2003, p. 17-22
8. D. Witkin, B.Q. Han, and E.J. Lavernia, Microstructural Evolution of an Ultrafine-Grained Cryomilled Al 5083 Alloy During Thermomechanical Processing, *J. Mater. Res.,* Vol 20, 2005 (submitted for publication)
9. G.E. Dieter, *Mechanical Metallurgy,* 2nd ed., McGraw-Hill, New York, 1976, p 1-774
10. F. Zhou, S.R. Nutt, C.C. Bampton, and E.J. Lavernia, Nanostructure in an Al-Mg-Sc Alloy Processed by Low-energy Ball Milling at Cryogenic Temperature, *Metall. Mater. Trans. A,* Vol 34, 2003, p 1985-1992
11. H.V. Atkinson and S. Davies, Fundamental Aspects of Hot Isostatic Pressing: An Overview, *Metall. Mater. Trans. A,* Vol 31, 2000, p 2981-3000
12. M.F. Ashby, Sintering and Hot Isostatic Pressing Diagrams, *Powder Metallurgy: An Overview,* I. Jenkins and J.V. Wood, Ed., The Institute of Metals, London, 1991, p 144-166
13. T.G. Nieh and J. Wadsworth, Hall-Petch Relation in Nanocrystalline Solids, *Scr. Metall. Mater.,* Vol 25, 1991, p 955-958
14. V. Yamakov, D. Wolf, and S.R. Phillpot, Deformation Mechanism Crossover and Mechanical Behavior in Nanocrystalline Materials, *Phil. Mag. Lett.,* Vol 83, 2003, p 385-393
15. H. Van Swygenhoven, M. Spaczer, and A. Caro, Microscopic Description of Plasticity in Computer-generated Metallic Nanophase Samples: A Comparison between Cu and Ni, *Acta Mater.,* Vol 47, 1999, p 3117-3126
16. V. Yamakov, D. Wolf, M. Salazar, S.R. Phillpot, and H. Gleiter, Length-Scale Effects in the Nucleation of Extended Dislocations in Nanocrystalline Al by Molecular Dynamics Simulation, *Acta Mater.,* Vol 49, 2001, p 2713-2722
17. C.J. Youngdahl, J.R. Weertman, R.C. Hugo, and H.H. Kung, Deformation Behavior in Nanocrystalline Copper, *Scr. Mater.,* Vol 44, 2001, p 1475-1478
18. D.G. Morris and M.A. Morri, Microstructure and Strength of Nanocrystalline Copper Alloy Prepared by Mechanical Alloying, *Acta Metall. Mater.,* Vol 39, 1991, p 1763-1770
19. S. Cheng, J.A. Spencer, and W.W. Milligan, Strength and Tension/Compression Asymmetry in Nanostructured and Ultrafine Grain Metals, *Acta Mater.,* Vol 51, 2003, p 4505-4818
20. R.W. Hayes, D. Witkin, F. Zhou, and E.J. Lavernia, Deformation and Activation Volumes for Cryomilled Ultrafine-grained Aluminum, *Acta Mater.,* Vol 52, 2004, p 4259-4271
21. W.W. Milligan, Mechanical Behavior of Bulk Nanocrystalline and Ultrafine-grain Metals, *Interfacial and Nanoscale Fracture,* W. Gerberich and W. Yang, Ed., Elsevier Pergamon, Amsterdam, 2003, p 529-550
22. H. Conrad and J. Narayan, Mechanisms for Grain Size Hardening and Softening in Zn, *Acta Mater.,* Vol 50, 2002, p 5067-5078
23. H. Conrad, Grain Size Dependence of the Plastic Deformation Kinetics in Cu, *Mater. Sci. Eng. A,* Vol 341, 2003, p 216-228
24. Q. Wei, S. Cheng, K.T. Ramesh, and E. Ma, Effect of Nanocrystalline and Ultrafine Grain Sizes on the Strain Rate Sensitivity and Activation Volume: FCC versus BCC Metals, *Mater. Sci. Eng. A,* Vol 381, 2004, p 71-79
25. G.T.I. Gray, T.C. Lowe, C.M. Cady, R.Z. Valiev, and I.V. Aleksandrov, Influence of Strain Rate and Temperature on the Mechanical Response of Ultrafine-grained Cu, Ni, and Al-4.0Cu-0.5Zr, *Nanostruct. Mater.,* Vol 9, 1997, p 477-480
26. T. Mukai, S. Suresh, K. Kita, H. Sasaki, N. Kobayashi, K. Higashi, and A. Inou, Nanostructured Al-Fe Alloys Produced by E-Beam Deposition: Static and Dynamic Tensile Properties, *Acta Mater.,* Vol 51, 2003, p 4197-4208
27. D.J. Skinner, M.S. Zedalis, and P.S. Gilman, Effect of Strain Rate on Tensile Ductility for a Series of Dispersion-strengthened Aluminum-based Alloys, *Mater. Sci. Eng. A,* Vol 119, 1989, p 81-86
28. S. Mitra, Elevated Temperature Mechanical Properties of a Rapidly Solidified Al-Fe-V-Si Alloy, *Scr. Mater.,* Vol 27, 1992, p 521-526
29. D.J. Lloyd, The Deformation of Commercial Aluminum-Magnesium Alloys, *Metall. Trans. A,* Vol 11, 1980, p 1287-1294
30. Y.M. Wang and E. Ma, Strain Hardening, Strain Rate Sensistivity and

Ductility of Nanostructured Metals, *Mater. Sci. Eng. A,* Vol 375-377, 2004, p 46-52
31. E.A. Brandes, *Smithells Metals Reference Book* 7th ed., E.A. Brandes and G.B. Brook, Ed., Butterworth Heineman, Oxford, 1992, p 13-45
32. H.J. Frost and M.F. Ashby, *Deformation-Mechanism Maps,* Vol 1, Pergamon Press, New York, 1982, p 1-166
33. A.R.C. Westwood and T. Broom, Strain-Aging of Aluminum-Magnesium Alloys at Temperatures between 208 and 369 K., *Acta Metall.,* Vol 5, 1957, p 249-256
34. E.O. Hall, *Yield Point Phenomena in Metals and Alloys,* MacMillan and Company, London, 1970, p 1-296
35. J.E. King, C.P. You, and J.F. Knot, Serrated Yielding and the Localized Shear Failure Mode in Aluminum Alloys, *Acta Metall.,* Vol 29, 1981, p 1553-1566
36. U.F. Kocks and H. Meckin, Physics and Phenomenology of Strain Hardening: The FCC Case, *Prog. Mater. Sci.,* Vol 48, 2003, p 171-273
37. W.J.M. Tegart, Role of Ductility in Hot Working, *Ductility,* ASM International, 1968, p 143-177
38. X. Zhang, H. Wang, R.O. Scattergood, J. Narayan, C.C. Koch, A.V. Sergueeva, and A.K. Mukherjee, Tensile Elongation (110%) Observed in Ultrafine-grained Zn at Room Temperature, *Appl. Phys. Lett.,* Vol 81, 2002, p 823-825
39. A.K. Ghosh and R. Raj, Grain Size Distribution Effects in Superplasticity, *Acta Metall.,* Vol 29, 1981, p 607-616
40. Y. Wang, M. Chen, F. Zhou, and E. Ma, High Tensile Ductility in a Nanostructured Metal, *Nature,* Vol 419, 2002, p 912-915
41. Y. Wang and E. Ma, Three Strategies to Achieve Uniform Tensile Deformation in a Nanostructured Metal, *Acta Mater.,* Vol 52, 2004, p 1699-1709
42. R.W. Hayes, R. Rodriguez, and E.J. Lavernia, The Mechanical Behavior of a Cryomilled Al-10Ti-2Cu, *Acta Mater.,* Vol 49, 2001, p 4055-4068
43. J.P. Hirth and J. Lothe, *Theory of Dislocations,* 2nd ed., John Wiley and Sons, New York, 1982, p 1-857